2013

Magnetism of rapidly quenched rhombohedral Zr_2Co_{11}-based nanocomposites

Wenyong Zhang
University of Nebraska-Lincoln, wenyong.zhang@unl.edu

Xingzhong Li
University of Nebraska-Lincoln, xli2@unl.edu

Shah R. Valloppilly
University of Nebraska-Lincoln, svalloppilly2@unl.edu

Ralph A. Skomski
University of Nebraska-Lincoln, rskomski2@unl.edu

Jeffrey E. Shield
University of Nebraska - Lincoln, jshield@unl.edu

See next page for additional authors

Published in *Journal of Physics D: Applied Physics* 46:13 (2013), 135004 (5 pp.); doi:10.1088/0022-3727/46/13/135004

Submitted October 10, 2012; revised January 27, 2013; published March 5, 2013.

Magnetism of rapidly quenched rhombohedral Zr_2Co_{11}-based nanocomposites

W. Y. Zhang,[1,2] X. Z. Li,[2] S. Valloppilly,[2] R. Skomski1,[2] J. E. Shield,[2,3] and D. J. Sellmyer[1,2]

1. Department of Physics and Astronomy, University of Nebraska, Lincoln, NE 68588, USA
2. Nebraska Center for Materials and Nanoscience, University of Nebraska, Lincoln, NE 68588, USA
3. Department of Mechanical and Materials Engineering, University of Nebraska, Lincoln, NE 68588, USA

Corresponding author – W. Y. Zhang, email wenyong.zhang@unl.edu

Abstract

The effect of quench rate and Zr content on nanostructure and magnetic properties of melt-spun Zr_xCo_{100-x} (x = 16–21) is investigated. High quench rate favors the formation of rhombohedral Zr_2Co_{11}, which is the hard phase. The coercivity increases with an increase in quench rate. Zr addition in limited amounts decreases the grain size of magnetic phases, which may promote the effective exchange coupling of soft magnetic phases. Therefore, coercivity and maximum energy product of Zr_2Co_{11}-based materials are significantly enhanced. The best magnetic properties, ${}_iH_c$ = 3.0 kOe and $(BH)_{max}$ = 4.6 MG Oe, which are the highest reported values among Co–Zr binary alloys, are achieved for x = 18. The temperature coefficients of coercivity and remanence between 100 and 380 K are −0.05% K^{-1}, comparable to those of alnico magnet.

1. Introduction

Zr_2Co_{11}-based alloys are promising candidates for developing a rare-earth-free permanent-magnet material due to high uniaxial anisotropy (11 Merg cm^{-3}) and Curie temperature (500°C).[1,2] Their magnetic properties are superior to those of sintered ferrite. The stoichiometry can be denoted as $ZrCo_{5.5-y}$ where y typically is 0.4.[3] Depending on the preparation

process, the crystal structure of Zr_2Co_{11} may be pseudohexagonal, rhombohedral, or orthorhombic.[4–6] Until now, the structure that leads to hard magnetism is under dispute. Recently, most work was focused on optimizing nanostructure and improving the magnetic properties of Zr_2Co_{11}-based alloys.[7–9] The phase component of the Zr–Co alloy was found to be strongly dependent on Zr content.[3] However, how Zr addition affects nanostructure and magnetic properties of the nanocrystalline Zr–Co alloy is unclear. It is known that melt spinning is a good way to fabricate metastable phases and develop fine nanostructure because of its very high quench rate. In this paper, we study how wheel speed and Zr content affect nanostructure and magnetic properties of melt-spun Zr–Co alloys. The experimental results show that hard magnetism arises from the rhombohedral Zr_2Co_{11}. Its volume fraction is closely related to the wheel speed and Zr content. High wheel speed helps one to form rhombohedral Zr_2Co_{11}. Proper Zr addition optimizes the nanostructure of melt-spun Zr–Co alloys, and this leads to enhancement of coercivity and energy product. The optimum magnetic properties were obtained for $x = 18$.

2. Experimental methods

Ingots of Zr_xCo_{100-x} (x = 16, 17, 18, 19, 21) were arc melted from high-purity elements in an argon atmosphere. The ribbons were made by ejecting molten alloys in a quartz tube onto the surface of a copper wheel with speeds from 5 to 60 m s^{-1}. The process parameters such as ejection pressure, diameter of the quartz tube hole, melting time, and distance between quartz tube and the surface of copper wheel were optimized for obtaining high-quality ribbons. The ribbons are about 2 mm wide and 50 μm thick. The phase components were examined by Rigaku D/Max-B x-ray diffraction (XRD) with Cu Kα radiation. The nanostructure was observed by JEOL 2010 transmission electron microscope (TEM). The hysteresis loops were measured by a superconducting quantum interference device (SQUID) magnetometer at fields up to 7 T. The phase components were estimated by thermomagnetic measurements using a physical property measurement system (PPMS) at temperatures up to 1000 K. The phase components for Zr_xCo_{100-x} (x = 16, 18, 21) at 45 m s^{-1} are listed in table 1. The applied field is parallel to the long direction of the ribbon.

Table 1. Phase component of Zr_xCo_{100-x} (x = 16, 18, 21) at 45 m s^{-1}

Zr_xCo_{100-x}	Co (vol%)	Zr_2Co_{11} (vol%)	Zr6Co23 (vol%)
16	7	89.6	3.4
18	4.6	90.4	5
21	1.5	86	12.5

3. Results and discussion

Figure 1(a) shows XRD patterns of Zr_xCo_{100-x} (x = 16, 18, and 21) at 25 m s^{-1}. The diffraction peaks of all the samples are indexed to the rhombohedral Zr_2Co_{11}, orthorhombic Zr_2Co_{11}, fcc Co, and cubic Zr6Co23 phases in good agreement with the results of thermomagnetic measurement. The relative intensity of the main diffraction peak for orthorhombic Zr_2Co_{11}

and Co decreases with increasing x. This indicates that the content of Co and orthorhombic Zr_2Co_{11} decrease with x. It is supposed that the volume fraction of rhombohedral Zr_2Co_{11} increases with x. For $x > 18$, the volume fraction of Zr6Co23 increases with x. This may lead to the reduction of the content of rhombohedral Zr_2Co_{11}. The largest amount of rhombohedral Zr_2Co_{11} may be achieved for $x = 18$. Figure 1(b) shows XRD patterns of $x = 16$ at 15, 25, and 45 m s^{-1}. It is evident that the relative intensity of the diffraction peak for the rhombohedral Zr_2Co_{11} in $x = 16$ increases with the increase in the wheel speed, indicating the higher volume fraction of this phase. In addition, according to the Scherrer equation, the estimated mean grain size of Zr_2Co_{11} decreases from 60 nm for 15 m s^{-1} to 30 nm for 45 m s^{-1}. These results indicate that higher wheel speed leads to a finer grain size of the magnetic phases.

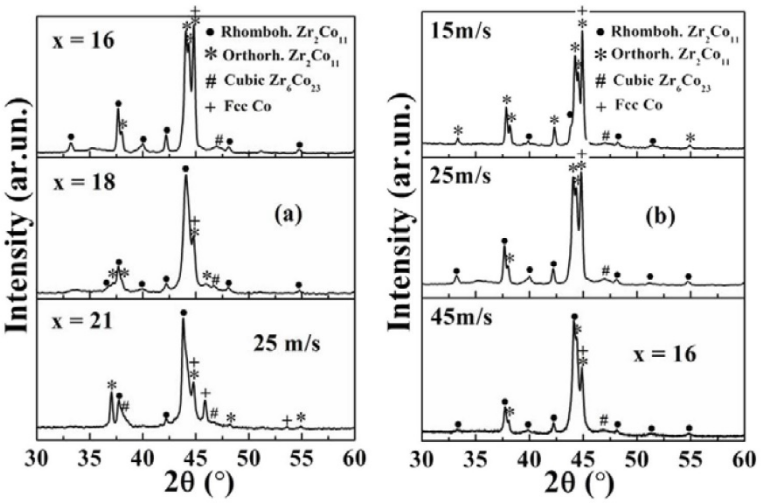

Figure 1. XRD patterns of Zr_xCo_{100-x} ribbons (a) $x = 16$, 18, 21 at 25 m s^{-1} and (b) $x = 16$ at 15 m s^{-1}, 25 m s^{-1}, 45 m s^{-1}.

Figures 2(a)–(c) show typical TEM images of the Zr_xCo_{100-x} ($x = 16$, 18, 21) ribbons with wheel rotating speed of 45 m s^{-1}. The grain size distribution (see figs. 2(d)–(f)) shows the mean grain size of the soft phase for $x = 16$, 18, and 21 are 90 nm, 60 nm, and 75 nm, respectively. The average grain size of the hard phase for $x = 16$, 18 and 21 are 210 nm, 140 nm and 180 nm, respectively. This indicates that proper Zr addition refines the grain size of the soft phase. Excessive Zr addition coarsens the grain size. Figures 2(g)–(i) show selected-area electron diffraction (SAED) patterns of the TEM specimen from the ribbons ($x = 18$). Figure 2(g) shows the SAED pattern of the rhombohedral Zr_2Co_{11} phase with the zone axis [1 1 0]. The basic reflections (0 0 3) and (3–3 0) are labeled in the SAED pattern. Figure 2(h) shows the SAED pattern of the orthorhombic Zr_2Co_{11} phase with the zone axis [0 1 0]. The reflections (0 0 3 0) and (2 0 0) are labeled in the SAED pattern. As shown in table 2, two sets of lattice parameters were reported.[5,6] Figure 2(e) was indexed according to the lattice parameters reported by Demczyk and Cheng.[6] Figure 2(i) shows the cubic

Zr_6Co_{23} phase with a zone axis of [0 0 1]. The electron diffraction analysis is in good agreement with the XRD results discussed above. The identification of the above phases verifies the XRD results.

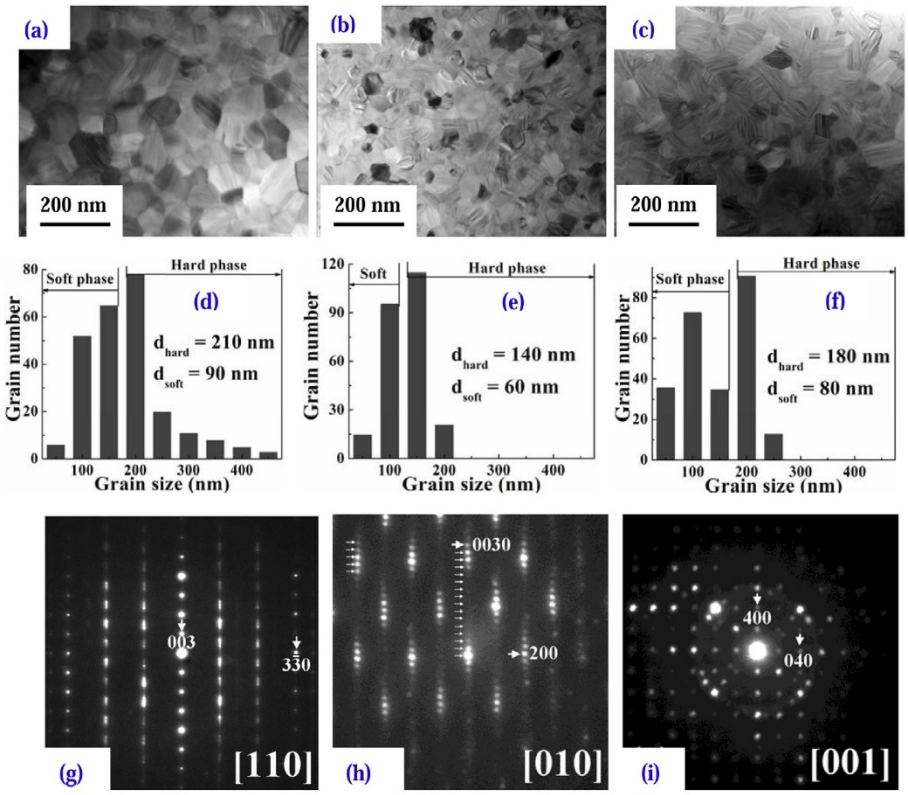

Figure 2. TEM images of Zr_xCo_{100-x} ribbons (a) x = 16 at 45 m s^{-1}, (b) x = 18 at 45 m s^{-1}, (c) x = 21 at 45 m s^{-1}, grain size statistical distribution of (d) x = 16 at 45 m s^{-1}, (e) x = 18 at 45 m s^{-1}, (f) x = 21 at 45 m s^{-1}, and (g), (h), (i) typical SAED patterns of x = 18 at 45 m s^{-1}.

Table 2. Crystallographic data of the Zr_2Co_{11} and Zr_6Co_{23} phases

Phase	Composition	Lattice (nm)	References
HT metastable	Zr_2Co_{11}	Rhombohedral a = 0.476 b = 2.420	[5]
LT metastable	Zr_2Co_{11}	Orthorhombic a = 0.471 b = 1.670 c = 2.420	[5, 6]
		Orthorhombic a = 0.480 b = 0.820 c = 3.600	
Equilibrium	Zr_6Co_{23}	Cubic a = 1.152	[12]

Note: HT is high temperature, LT is low temperature.

Figures 3(a)–(c) show typical hysteresis loops of Zr_xCo_{100-x} with different wheel speeds, various Zr Content and deduced magnetic property dependence on x, respectively. The saturation magnetization of x = 16 is almost unchanged with the increase in the wheel speed. The coercivity increases from 0.6 kOe at 15 m s^{-1} to 1.7 kOe at 45 m s^{-1} most likely

due to the finer grain size of magnetic phases and the higher volume fraction of the rhombohedral Zr_2Co_{11}. The demagnetization curves for Zr_xCo_{100-x} (x = 16, 18, 21) at 45 m s^{-1} show a single hard magnetic phase behavior, indicating the existence of strong interphase exchange coupling. The saturation field of all the ribbons is about 35 kOe and unrelated to Zr content. The saturation magnetization decreases with x possibly due to the increase in Zr_6Co_{23} content with a low magnetization. Proper Zr addition leads to a significant increase in remanence ratio and coercivity. This is attributed to the grain size refinement of magnetic phases and the increase in the hard phase content (see fig. 2 and table 1), which promote the effective exchange coupling of the soft phase. Excessive Zr addition may decrease the content of rhombohedral Zr_2Co_{11}, which lowers the remanence and worsens the squareness (SQ) of the demagnetization curves. Therefore, the maximum energy product decreases with x. The best maximum energy product, which is twice larger than reported value among binary Zr–Co alloys, was attained for x = 18. It was reported that the saturation magnetization of Zr_2Co_{11}-based alloys increases linearly when cobalt is replaced by iron.[2] Thus, the magnetic properties of the x = 18 may be further improved by adding Fe or decreasing the grain size of soft magnetic phases to the order of the domain-wall thickness.

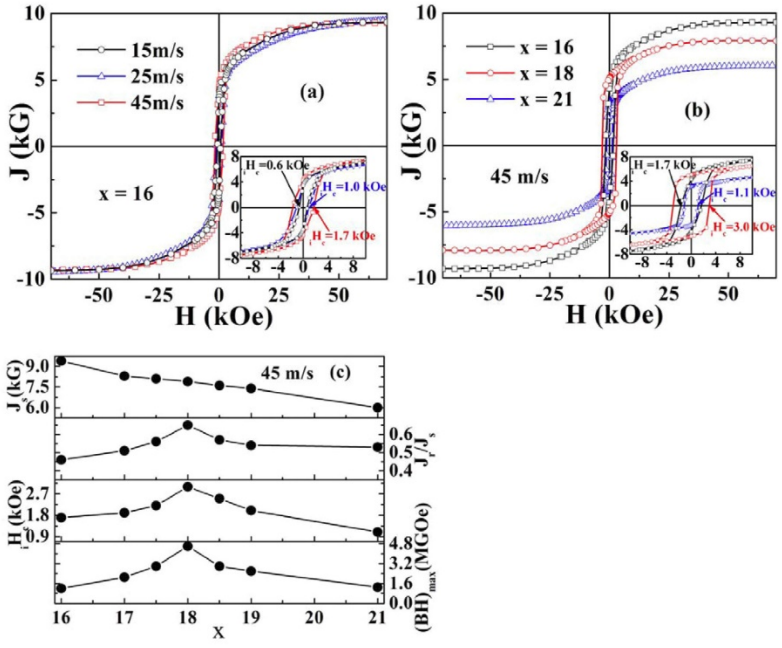

Figure 3. Room-temperature hysteresis loops of Zr_xCo_{100-x} ribbons (a) x = 16 at 15, 25, and 45 m s^{-1}, (b) x = 16, 18, and 21 at 45 m s^{-1}, and (c) deduced magnetic properties.

Figure 4 shows demagnetization curves at various temperatures of x = 18. The temperature coefficients of remanence α and coercivity β are defined as $\alpha = \{[M_r(T_0) - M_r(T_1)]/[M_r(T_0) \times (T_0 - T_1)]\} \times 100\%$; $\beta = \{[{}_iH_c(T_0) - {}_iH_c(T_1)]/[{}_iH_c(T_0) \times (T_0 - T_1)]\} \times 100\%$, where $150 \le T_1 \le 380$ K and T_0 = 100 K. α and β values of the sample are the same, −0.05% K^{-1}, which is

close to that of alnico magnet. The SQ of the demagnetization curves can be defined as the ratio of $|H(M/M_r = 90\%)/H_c|$. The value of SQ at 100 K and 380 K is 0.42 and 0.41, respectively. They are almost unchanged with the increase in temperature, as shown in the lower right inset. This reflects that the exchange correlation length (ECL) among magnetic phases is almost unchanged down to 100 K. Generally, ECL corresponds to the domain wall width of the hard magnetic phase, $2\pi(A/K)^{1/2}$, where A and K are the exchange constant and the magnetocrystalline anisotropy parameter of the hard magnetic phase, respectively.[10] Therefore, it is concluded that K slightly changes with the decrease in temperature. K can be estimated by fitting the high-field magnetization measurements to the following expression:[11]

$$M(H) = M_s[1 - A/H^2] + \chi H \quad (1)$$

$$A = 4K^2/15M^2_s, \quad (2)$$

where M_s is the spontaneous magnetization, χ is the high-field susceptibility and K is magnetocrystalline anisotropy constant. The results obtained from the best fit are shown in the upper left inset. The K values at 100 K and 380 K are 14 Mergs cm^{-3} and 11 Mergs cm^{-3}, respectively, in good agreement with the previous deduction that K slightly changes with the decrease in temperature.

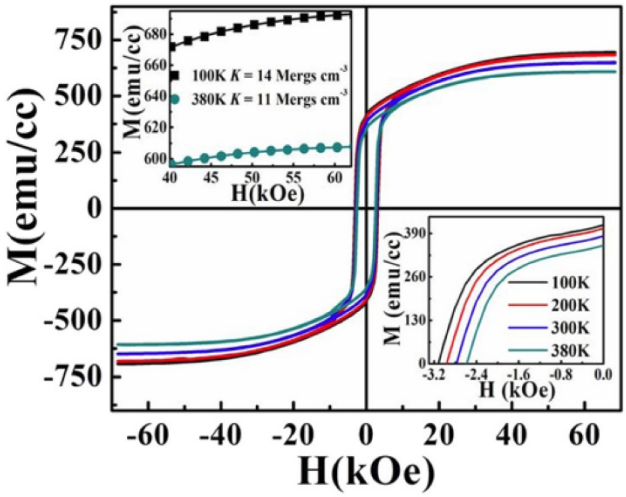

Figure 4. Hysteresis loops at various temperature of Zr_xCo_{100-x} ribbons (x = 18) at 25 m s^{-1}.

4. Conclusions

In summary, structure-property relationships of melt-spun Zr_2Co_{11}-based materials have been analyzed. The hard magnetism results from the rhombohedral Zr_2Co_{11} phase. Its volume fraction may be tuned by varying the wheel speed or Zr content. Increasing wheel speed promotes the formation of rhombohedral Zr_2Co_{11}, and thus improves magnetic properties. Proper Zr addition refines the grain size of magnetic phases. As a result, the

volume fraction of exchange-coupled soft phases increases. Therefore, coercivity and energy product are significantly enhanced. The maximum energy product, comparable to cast alnico magnets, is obtained for $x = 18$. This material has α and β values of -0.05% K^{-1} between 100 and 380 K, which are much lower than that of sintered $Nd_2Fe_{14}B$ magnets. The properties reported above are for a granular material with random anisotropy axes. If alignment of these axes can be achieved, the resulting energy product can be enhanced further.

Acknowledgments – The authors would like to thank Mrs. Xiujuan-Hellen Jiang and Mr. Bhaskar Das for assistance in sample preparation. This work is supported by DOE/Ames/BREM under grant DE-AC02-07CH11358, and NCMN.

References

[1] Ishikawa T and Ohmori K 1990 *IEEE Trans. Magn.* 26 13704.

[2] Burzo E, Grössinger R, Hundegger P, Kirchmayr H R, Krewenka R, and Lemaire R 1991 *J. Appl. Phys.* 70 6550.

[3] Gabay A M, Zhang Y, and Hajipanayis G C 2001 *J. Magn. Magn. Mater.* 236 37.

[4] Stadelmaier H H, Jang T S, and Henig E-Th 1991 *Mater. Lett.* 12 295.

[5] Ivanova G V, Shchegoleva N N, and Gabay A M 2007 *J. Alloys Compounds* 432 135.

[6] Demczyk B G and Cheng S F 1991 *J. Appl. Cryst.* 24 1023.

[7] Ghemawat A M, Foldeaki M, Dunlap R A. and O'Handley R C 1989 *IEEE Trans. Magn.* 25 3312.

[8] Zhang J B, Sun Q W, Wang W Q, and Su F 2009 *J. Alloys Compounds* 474 48.

[9] Stroink G, Stadnik Z M, Viau G, and Dunlap R A 1990 *J. Appl. Phys.* 67 49–63.

[10] Zhao T, Xiao Q F, Zhang Z D, Dahlgren M, Grössinger R, Buschow K H J, and Boer de F R 1999 *Appl. Phys. Lett.* 75 22–98.

[11] Hadjipanayis G C, Sellmyer D J, and Brandt B 1981 *Phys. Rev.* B 23 33–49

[12] Kuz'ma Y B, Markiv V Y, Voroshilov Y V, and Skolozdra R V 1966 *Inorg. Mater.* (Engl. Transl.) 2 22–25.